

Study of Transformer Resonant Overvoltages Caused by Cable-Transformer High-Frequency Interaction

Bjørn Gustavsen, *Senior Member, IEEE*

Abstract—Power transformers can fail from dielectric stresses caused by electromagnetic transients. In this paper, we focus on a special phenomenon where excessive overvoltages arise due to resonance. This situation can take place when a transformer on the high-voltage side is connected to a cable and the low-voltage side is unloaded. Very high overvoltages can then result on the low-voltage side from transient events that cause a weakly attenuated overvoltage on the cable with a dominant frequency matching a resonance peak in the transformer voltage ratio. Laboratory tests on a 11-kV/230 V distribution transformer show that a step voltage excitation on a 27-m cable produces 24-p.u. overvoltage on the open low-voltage side. The voltage waveforms are accurately reproduced by a black-box model obtained from frequency sweep measurements. Simulations show that overvoltages as high as 43 p.u. could occur with the most unfavorable cable length. It is further shown that the following situations can lead to high overvoltages on an unloaded transformer low-voltage side: 1) ground fault initiation at the far cable end, 2) cable energization from a busbar with several other cables connected, 3) cable energization from another cable with the same length, and 4) capacitor bank energization at the far cable end.

Index Terms—Cable, overvoltage, resonance, transformer.

I. INTRODUCTION

TRANSFORMERS can suffer dielectric failure due to high-frequency network-initiated transients, such as switching operations and fault events, as well as atmospheric discharges. One example was reported in [1] where a generator step-up transformer failed with bus fault as probable cause. The increasing number of transformer dielectric failures in later years has motivated CIGRE to initiate (2008) a new Working Group (A2/C4.39) whose scope of work includes assessing types of electrical transient interaction between the transformer and network.

Many studies have analyzed the dielectric stresses that can occur in transformer windings [2]–[8]. The calculation of these internal overvoltages requires a detailed geometrical description of the transformer. Since this information is normally proprietary to the manufacturer, these analyses are, in practice, difficult to carry out. In addition, the model's sensitivity to geometry

Manuscript received May 05, 2009; revised December 01, 2009. First published February 17, 2010; current version published March 24, 2010. This work was supported in part by the Norwegian Research Council (PETROMAKS Programme), in part by Aker Solutions, in part by Compagnie Deutsch, in part by FMC Technologies, in part by Framo, in part by Nexans, in part by Oceaneering Multiflex, in part by Petrobras, in part by Siemens, in part by StatoilHydro, in part by Total, and in part by Vetco Gray. Paper no. TPWRD-00340-2009.

The author is with SINTEF Energy Research, Trondheim N-7465, Norway (e-mail: bjorn.gustavsen@sintef.no).

Color versions of one or more of the figures in this paper are available online at <http://ieeexplore.ieee.org>.

Digital Object Identifier 10.1109/TPWRD.2010.2040292

and material properties makes it hard to achieve a high level of accuracy.

It is also useful to assess the external overvoltages on transformers. The transfer of lightning overvoltages between windings has been studied in [9]–[12] and shows, by principle, that energizing an unloaded transformer via a cable may cause excessive overvoltages on the secondary side due to a resonant overvoltage phenomenon. For the calculation of external overvoltages, black-box-type models [8]–[10], [13]–[17] are usually preferred as they do not require information about the transformer geometry and because they are capable of reproducing the transformer terminal behavior with a high degree of accuracy. These models are ideally suited for investigating how a transformer will behave when placed in a given network since it allows directly simulating the transient interaction between the network and the transformer. Black-box models are usually obtained from frequency sweep measurements at the transformer terminals followed by rational function approximation. The rational fitting process is often based on some variant of the vector fitting method [18] followed by perturbation [19] to enforce passivity. Such models can be easily interfaced with EMTP-type simulation programs [20] via a lumped electrical network [13], or by numerical integration of the state equations [21], [22].

The objective of this paper is to 1) show that black-box models are capable of representing the resonant overvoltage phenomenon with adequate accuracy and 2) identify situations which can cause excessive (external) resonant overvoltages. The study is based on laboratory measurements on an 11-kV/230 V distribution transformer that is connected to a (feeder) cable on the high-voltage side. Application of a step voltage to the cable results in a resonant overvoltage on the open low-voltage side. This situation corresponds to ground fault initiation on the cable. The overvoltage waveforms are compared to those obtained via simulations using a black-box model of the transformer and the cable. Using the obtained transformer model, the maximum transformer overvoltage is calculated with alternative cable lengths, and with alternative loadings on the low-voltage side. Finally, the level of resonant overvoltages is investigated for three other important situations. Energization is via the feeder cable from a busbar which is connected to several other cables, energization is via the feeder cable from another cable of equal length, and capacitor bank energization at the far end of the feeder cable.

II. TRANSFORMER RESONANT OVERVOLTAGES

A. Resonance Overvoltage Phenomenon

References [11] and [12] describe a so-called resonant overvoltage phenomenon that can lead to the magnification of transient voltages. The phenomenon can be understood from the cir-

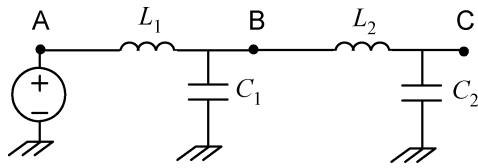
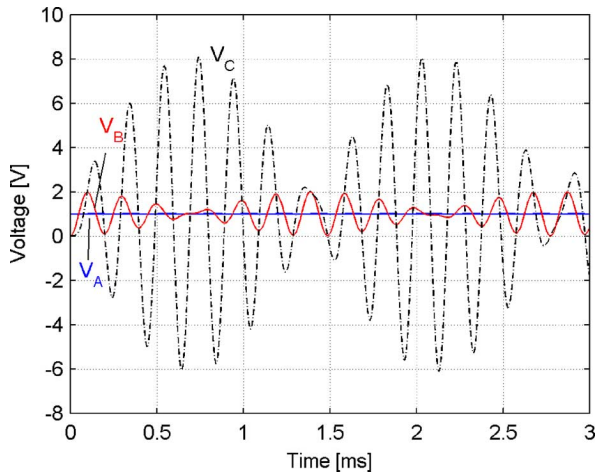


Fig. 1. Two series-connected RLC circuits.

Fig. 2. Unit step voltage excitation. Voltage at points A, B, and C in Fig. 1. $L_1 = 1$ mH, $C_1 = 1$ μ F, $L_2 = 50$ mH, $C_2 = 0.02$ μ F.

circuit in Fig. 1. The circuit formed by L_1 and C_1 is excited by a unit step voltage, giving rise to an oscillating voltage at B with frequency $\omega_1 = 1/\sqrt{L_1 C_1}$. A second circuit is next connected to point B, formed by L_2 and C_2 . If the second circuit (circuit #2) has a resonance frequency $\omega_2 = 1/\sqrt{L_2 C_2}$, which is equal to or almost equal to ω_1 , and the surge impedance of circuit #2 is much higher than that of circuit #1, $\sqrt{L_2/C_2} \gg \sqrt{L_1/C_1}$, a resonant overvoltage phenomenon will take place. This is shown in Fig. 2 for a unit step voltage excitation. Energy is exchanged back and forth between the two circuits, causing the observed beat phenomenon. The voltage peak value in circuit #2 is higher than that of circuit #1, due to the smaller circuit values. From the energy relation $W = C_1 V_1^2/2 = C_2 V_2^2/2$, the peak value of the oscillating voltage component V_2 in circuit #2 is approximately $\sqrt{C_1/C_2}$, or 7.1 with the given circuit values. In Fig. 2, the voltage is accordingly seen to vary between -6 V and $+8$ V as it oscillates around the applied voltage ($+1$ V).

B. Resonance Between the Cable and Transformer

The voltage transfer between windings in a transformer undergoes a strong variation as function of frequency as the voltage transfer at high frequencies is not governed by ampere-winding balance. With increasing frequency, the flux in the iron core decreases and the voltage ratio becomes eventually defined by stray inductances and capacitances between winding turns and between windings. This results in resonance peaks in the voltage transfer from the high-voltage side to the low side, often becoming many times higher than the voltage ratio at the operating frequency (50 Hz/60 Hz). The impedance seen into the transformer terminals is usually much higher on the high-voltage side

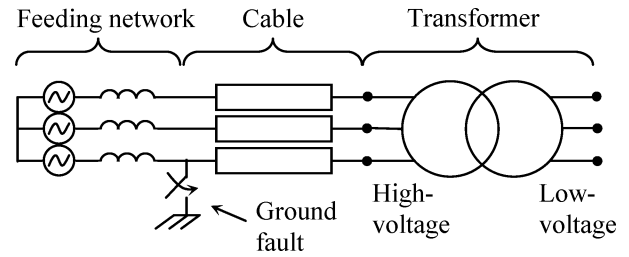


Fig. 3. Ground fault on the transformer high-voltage side. Single-phase drawing.

than on the low-voltage side (due to more turns), and it is particularly high in situations where the low-voltage winding is unloaded. Thus, high transformer external overvoltages are likely to occur if the following conditions are met as follows.

- 1) A transient occurs on the high-voltage side with the low-voltage side open or connected to a high-impedance load.
- 2) The transient has a dominating frequency which matches a resonance peak in the voltage transfer from high to low.
- 3) The input impedance seen into the high-voltage winding (with open low-voltage side) is sufficiently high so that the transformer loading effect does not appreciably reduce the voltage on the high-voltage side.

Note that these conditions resemble the resonant overvoltage condition described in Section II-A. In the following text, we describe four important cases that may produce high overvoltages on an unloaded transformer.

Case 1) Ground fault initiation (Fig. 3). If a ground fault occurs at the far end of the feeder cable which connects to the high-voltage side of an unloaded transformer, a coaxial wave starts propagating back and forth between the two cable ends. This results in an oscillating voltage on the cable end. Since the cable has a low characteristic impedance which, at high frequencies, can be much lower than that seen into the transformer high-voltage side, the transformer may lead to only a weak damping of the cable overvoltage. If the frequency of the cable resonant voltage coincides with a peak in the voltage transfer from the high-voltage side to the low-voltage side, very high overvoltages can result on the low-voltage side. This situation is similar to Fig. 1, with circuits #1 and #2 representing the cable and transformer, respectively.

Case 2) Cable energization (Fig. 4). If the feeder cable is switched to a busbar that is connected to several other cables, the impedance seen into the busbar from the feeder cable will be much lower than the cable characteristic impedance. The busbar will therefore appear as a low-impedance step voltage source and an oscillating voltage may appear on the transformer cable for a few cycles. High overvoltages can occur on the transformer low-voltage side due to resonance, similar to the ground fault case.

Case 3) Cable energization (Fig. 5). If the feeder cable is switched to a cable of the same length as the feeder cable, an oscillating voltage will occur on the cable

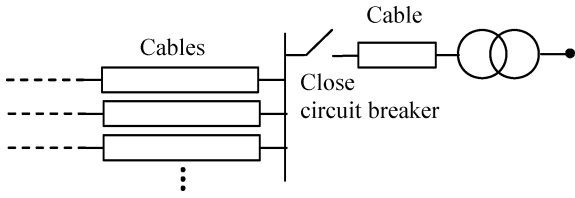


Fig. 4. Transformer energization via cable with the busbar connected to several cables. Three-phase drawing.

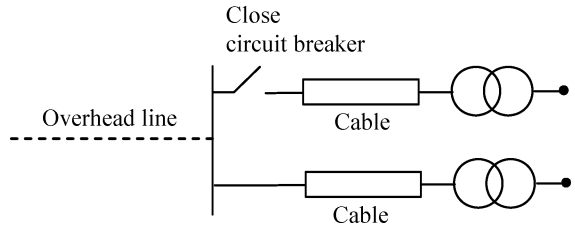


Fig. 5. Connecting two cables of equal length.

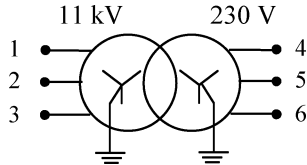


Fig. 6. The 300-kVA distribution transformer.

end with weak attenuation. Again, high overvoltages may result on the low-voltage side due to resonance.

Case 4) Capacitor bank energization. If a capacitor bank is switched to a busbar which is connected to the high-voltage side of an unloaded transformer via a cable, the voltage will initially drop to zero on the busbar and, hence, the cable end. This may cause high overvoltages on the transformer low-voltage side, similar as in the ground fault case.

These four cases will be subject to analysis by numerical simulation in Sections IV, V-A, V-B, and VI, respectively.

III. MODELING FOR DUPLICATING EXPERIMENTAL RESULTS

A. Transformer Modeling

The transformer is an 11-kV/230-V unit with 300-kVA rated power, connected as wye-wye with both neutrals grounded (see Fig. 6). The wideband modeling of this transformer will be reported in a different publication and we mention only the key issues. A network analyzer (Anritsu MS4630B) is used for measuring the terminal admittance matrix \mathbf{Y} in the range 10 Hz–10 MHz using a measurement setup similar to the one in [15]. The effect of the measurement cables is removed, giving a description with respect to the transformer's terminals. The admittance matrix is subjected to rational approximation by the model (1). The model is calculated by vector fitting [18], [24], [25] using 100 pole-residue terms in the range 50 Hz–10 MHz followed

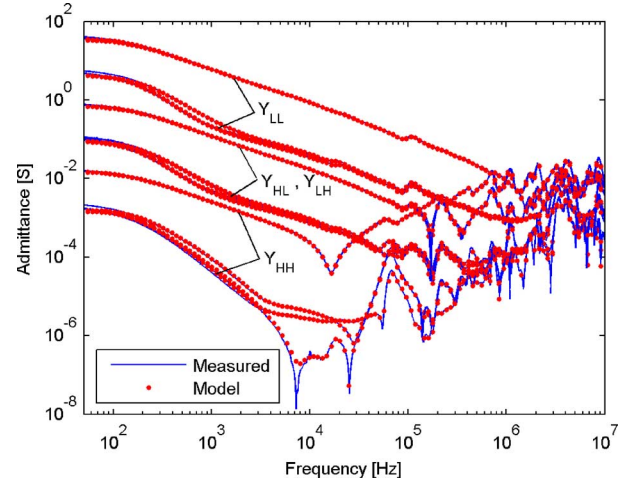


Fig. 7. Measured and fitted admittance matrix.

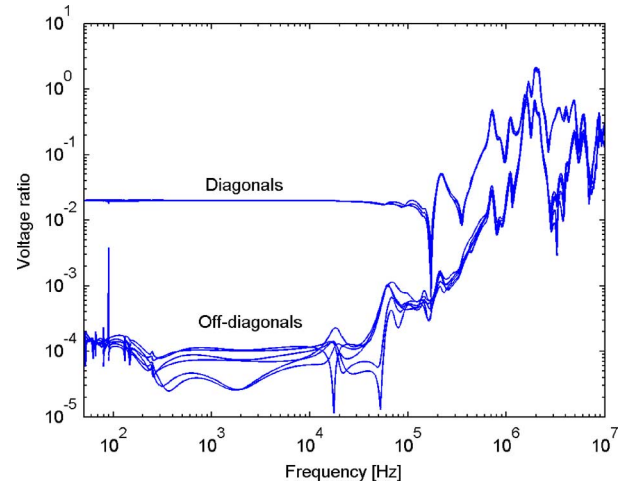


Fig. 8. Voltage ratio from high to low, computed from the model.

by passivity enforcement by residue perturbation [19], [26]. The model is symmetrical, causal, and has stable poles only

$$\mathbf{Y}(\omega) = \sum_{m=1}^N \frac{\mathbf{R}_m}{j\omega - a_m} + \mathbf{R}_0. \quad (1)$$

The measured admittance matrix and the rational fitting result is shown in Fig. 7. (Only a fraction of the samples is included in the plot of the model's response so that the negative spikes in the measurement are not well resolved.) The labels in the plot correspond to the matrix partitioning in (2)

$$\begin{bmatrix} \mathbf{i}_H \\ \mathbf{i}_L \end{bmatrix} = \begin{bmatrix} \mathbf{Y}_{HH} & \mathbf{Y}_{HL} \\ \mathbf{Y}_{LH} & \mathbf{Y}_{LL} \end{bmatrix} \begin{bmatrix} \mathbf{v}_H \\ \mathbf{v}_L \end{bmatrix}. \quad (2)$$

From the partitioning in (2), we obtain the voltage ratio \mathbf{H}_{LH} by (3). \mathbf{H}_{LH} is a 3×3 matrix which relates an applied voltage vector \mathbf{v}_H on the high-voltage side to the response \mathbf{v}_L on the open low-voltage side. The voltage ratio is shown in Fig. 8. It is observed that the voltage ratio at frequencies above 100 kHz is much higher than at 50 Hz. In principle, a 1-V stationary

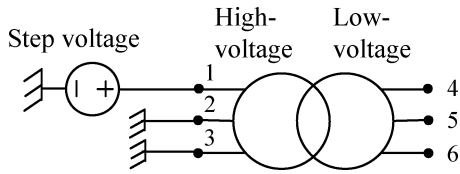


Fig. 9. Step voltage excitation.

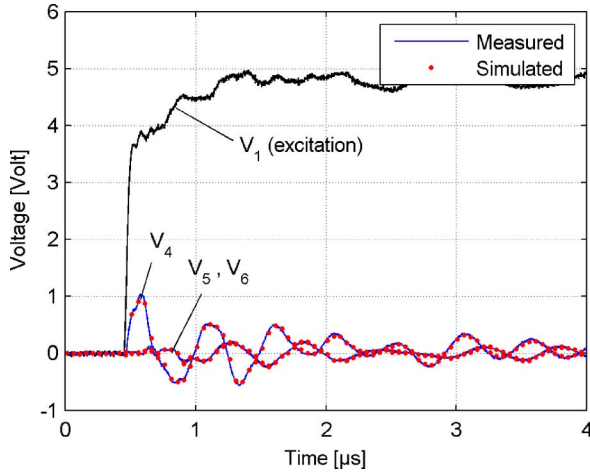


Fig. 10. Measured and simulated responses.

excitation on terminal #1 with terminals #2 and #3 grounded would give a voltage as high as 2 V on the low-voltage side

$$\mathbf{H}_{LH} = -\mathbf{Y}_{LL}^{-1} \mathbf{Y}_{LH}. \quad (3)$$

The time-domain counterpart of Fig. 8 can be found by exciting one of the high-voltage terminals with a step voltage with the other two terminals grounded (see Fig. 9). The resulting voltage responses on the low-voltage side correspond to one column of \mathbf{H}_{LH} . Fig. 10 shows that the measured voltage response at the low-voltage side has strong oscillations. In the same plot, the simulated voltage response is shown when the applied voltage (excitation) is realized as an ideal voltage source. The excellent agreement between measurement and simulation verifies the accuracy of the model. We also note that the 2-MHz component in the voltage transfer (Fig. 8) is observed in the time-domain response (Fig. 10).

B. Cable Modeling

A 240-mm² single-core 12-kV cable is to be connected to the transformer. Normally, cables are modeled by using a frequency-dependent traveling-wave model obtained from a geometry description [27], [28]. Since the high-frequency properties of the model are quite sensitive to inaccuracies in the cable geometry description, we will initially model the cable by using a measurement-based approach. That way, it becomes easier to focus on the accuracy of the transformer model. Later, we will use a model obtained via geometry for application studies with varying cable lengths.

Using frequency sweep measurements, the 2 × 2 admittance matrix \mathbf{Y} is obtained with respect to the two ends of a 27-m cable section, in the range 100 kHz–50 MHz. The admittance

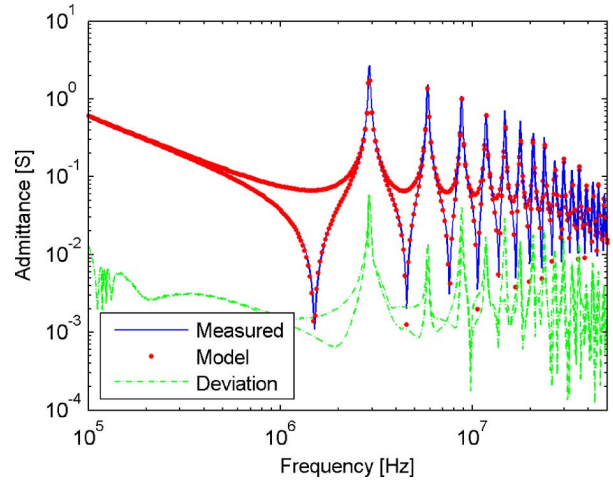


Fig. 11. Measured and fitted admittance matrix of the cable.

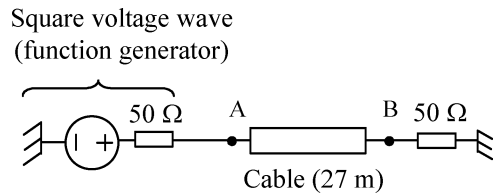


Fig. 12. Excitation of cable with the square voltage pulse with the far end grounded by a 50-Ω resistor.

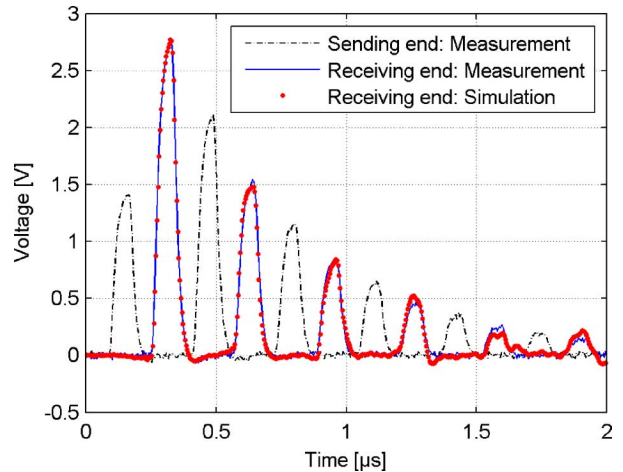


Fig. 13. Cable sending-end and receiving-end voltage.

matrix is obtained from the voltage ratio between the two cable ends, when the far end is either open-circuited or terminated by a 50-Ω resistor. The details are shown in the Appendix. Fig. 11 shows the obtained admittance matrix and its approximation by a rational model (1) obtained via vector fitting and passivity enforcement by residue perturbation.

In order to verify the accuracy of the cable model in the time domain, we apply a voltage pulse to one cable end (sending end) and measure the response at the receiving end which is terminated by a 50-Ω resistor, see Fig. 12. The applied voltage is taken as an ideal voltage source in a simulation of the voltage response at the receiving end. Fig. 13 compares the measured and simulated voltage at the receiving end, demonstrating very

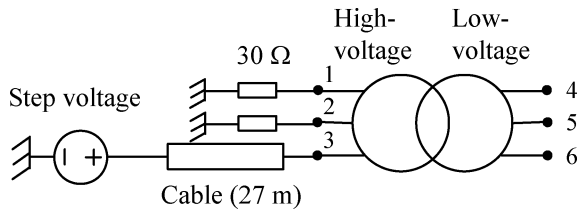


Fig. 14. System overview.

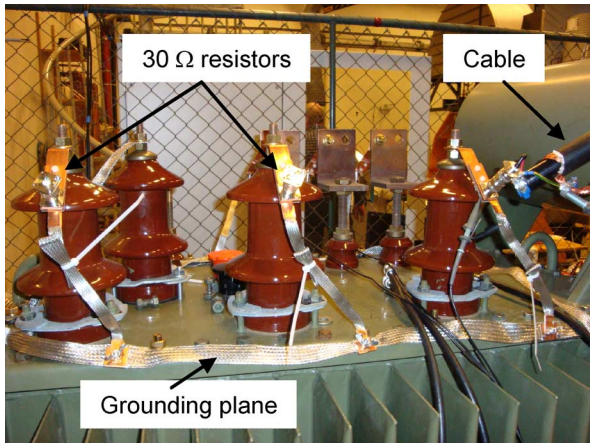


Fig. 15. Connections on the transformer.

good agreement. The oscillations occur because the cable characteristic impedance does not match the 50- Ω resistance of the source and the load. The good agreement implies that the cable model has the correct characteristic impedance and time delay.

IV. GROUND FAULT INITIATION ON THE FEEDER CABLE

In a laboratory experiment, we connect the cable to terminal #3 on the high-voltage side of the transformer, see Fig. 14. Terminals #1 and #2 are grounded through 30- Ω resistors, giving a loading impedance that is not much different from the cable characteristic impedance. The transformer low-voltage side is left open. A step voltage source with a very low internal impedance is connected to the sending end of the cable, thereby giving rise to a voltage oscillation on the cable. This situation is now similar to the ground fault situation in Fig. 3 in the sense that the transformer loading impedance is the main source of damping of the oscillating voltage on the cable. In the actual laboratory setup, the cable is connected by using very short connection leads so as to minimize the effect of parasitic inductances, see Fig. 15.

Fig. 16 shows the voltage on the cable at the sending end (excitation) and receiving end, before the transformer is connected. It is seen that the voltage oscillates with only very low attenuation. With the measured voltage at the sending end taken as an ideal voltage source in a simulation, the cable model is seen to reproduce the voltage response at the receiving end quite accurately.

Fig. 17 shows the same result as in Fig. 16, after connecting the transformer. It is seen that the transformer causes a significant attenuation of the remote end cable voltage (V_3). The voltage on terminals #5 and #6 on the low-voltage side (V_5 , V_6) is also shown in the plot. It is seen that the voltage on

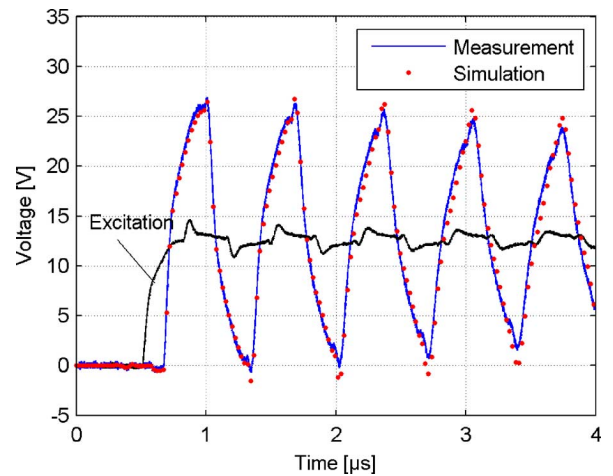


Fig. 16. Cable overvoltage at the sending end (excitation) and receiving end (measurement/simulation), with the disconnected transformer.

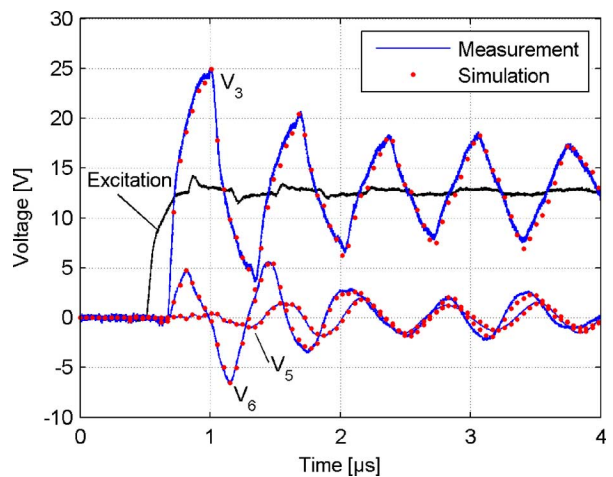


Fig. 17. Overvoltages with the connected transformer.

the low-voltage side reaches a value which is about 50% of the excitation voltage on the cable sending end. The voltage ratio of the transformer is 11000/230 (i.e., 48:1). This implies that the secondary voltage reaches a value of 24 p.u. of the normal phase-to-ground voltage. Thus, if the impinging voltage (sending end) was equal to the normal phase-to-ground voltage (i.e., 8.9 kV), the transient voltage on the 230-V side would reach 4.4 kV. The same plot also shows the simulated voltage waveforms with the cable sending end voltage taken as an ideal voltage source. The agreement with the measured quantities is seen to be excellent.

For comparison, the direct step voltage excitation in Fig. 10 (without cable) gave only a 12-p.u. overvoltage on the low-voltage side. The reason for higher voltage in Fig. 17 is the resonance between the cable and the transformer. In this case, the resonance leads to a doubling of the peak voltage, compared to a direct step voltage excitation.

We now wish to analyze the overvoltage with alternative cable lengths. To achieve this, the measurement-based cable model is replaced by a frequency-dependent traveling-wave-type model [28] where the electrical per-unit-length parameters (R , L , C) are obtained from the geometry description in Table I by using

TABLE I
CABLE DESCRIPTION

	Radius [mm]	Thickness [mm]	Resistivity [$\Omega \cdot \text{m}$]	ϵ_r
Phase conductor	9.25		$3.36E-8$	
Semiconductor		0.5		
Insulation		3.4		2.3
Semiconductor		0.5		
Sheath conductor		0.4	$1.72E-8$	
Jacket		2		2.3

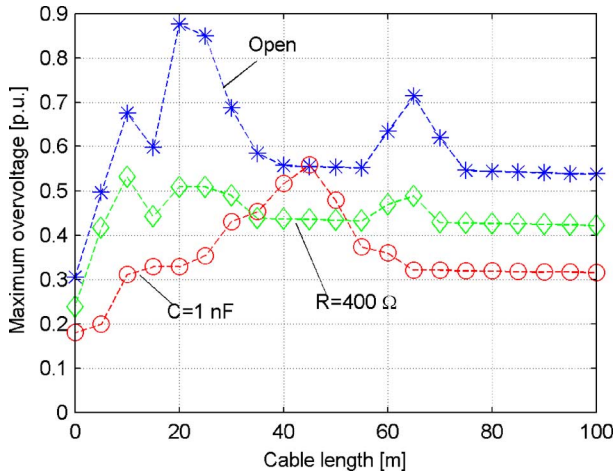


Fig. 18. Simulation of maximum overvoltage on the low-voltage side as a function of the cable length. The configuration in Fig. 14 shows the ideal step voltage excitation. The overvoltage is shown in per unit of applied voltage.

the procedure in [27]. The semiconducting layers are taken into account by replacing them with insulation while increasing the permittivity of the entire insulation slab (between conductor and sheath) from 2.3 to 3.0, following the procedure in [29].

Fig. 18 shows the maximum overvoltage on the low-voltage side for alternative cable lengths when the excitation is an ideal unit step voltage. With open low-voltage terminals, the maximum voltage peaks at 0.9 p.u. of the applied voltage for a 20-m cable. This corresponds to 43 p.u. of the normal (50-Hz) voltage. The corresponding simulation is shown in Fig. 19. It is seen that the cable voltage quickly decays as energy is transferred from the cable to the transformer, resulting in a strong increase of the transformer overvoltage. The similarity with the idealized result in Fig. 2 is striking.

Fig. 18 further shows that the overvoltage becomes strongly reduced if the low-voltage side is connected to even a small load. For reference, 400 Ω approximately corresponds to the characteristic impedance of an overhead line while 1 nF could represent the shunt capacitance effect of a 3-m cable stub.

The cable characteristic impedance is an essential parameter in the resonance overvoltage phenomenon. Fig. 20 shows the maximum overvoltage as a function of cable length with the cable characteristic impedance as the parameter. In these simulations, the cable is replaced with a lossless cable model, assuming a wave velocity of 177 m/ μs . It is seen that the maximum voltage is reduced as the characteristic impedance increases. The voltage reduction occurs because a higher characteristic impedance implies less energy stored in the cable and

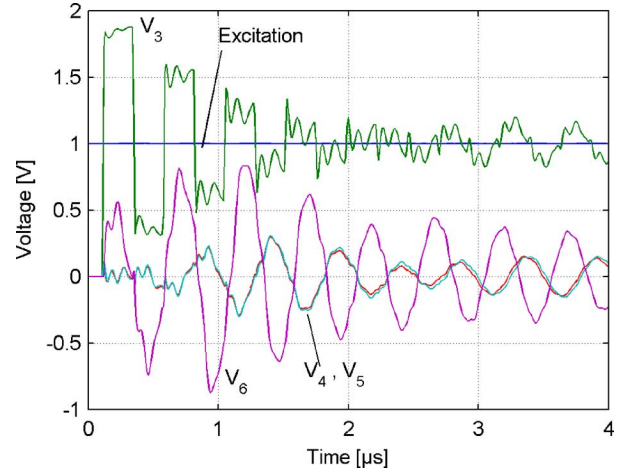


Fig. 19. Simulated step voltage response. 20-m cable.

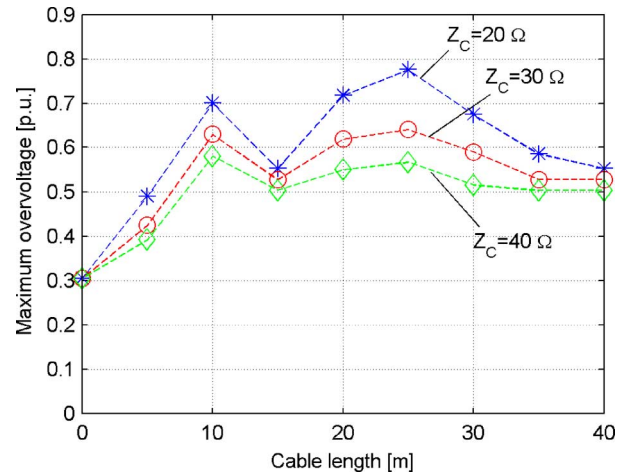


Fig. 20. Maximum overvoltage as function of cable length. Lossless cable with alternative values for characteristic impedance. Configuration in Fig. 14 with ideal step voltage excitation.

so the voltage oscillation on the cable decays faster, thereby reducing the voltage buildup on the low-voltage side.

V. TRANSFORMER ENERGIZATION VIA A FEEDER CABLE

A. Busbar Connected to Several Long Cables

As explained in Section II, high transformer overvoltages can also result if the transformer is energized via a (feeder) cable from a busbar that is connected to several other cables. An example of this is shown in Fig. 21. The busbar is connected to four cables in addition to the 20-m feeder cable. When the circuit breaker closes with a voltage V_{bus} on the busbar, the resulting voltage at the instant following breaker contact becomes $V_{\text{bus}} \cdot (4/5) = 0.8 V_{\text{bus}}$, when assuming that all cables have an identical characteristic impedance. In this simulation, a frequency-dependent cable model is used, based on the data in Table I with 0.5-m separation between the three single-core cables.

Fig. 22 shows a time-domain simulation of this situation. It is assumed that the phase C breaker closes 1 ms before the next breaker, and that the voltage is maximum in phase C. The plot

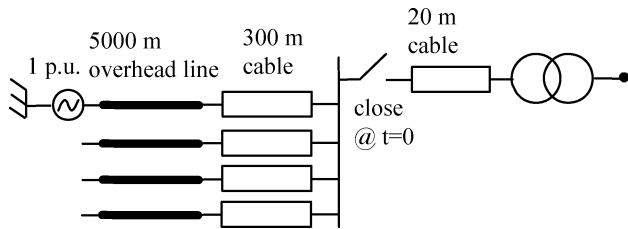


Fig. 21. Transformer energization from the three-phase power system. Closing first breaker pole at $t = 0$.

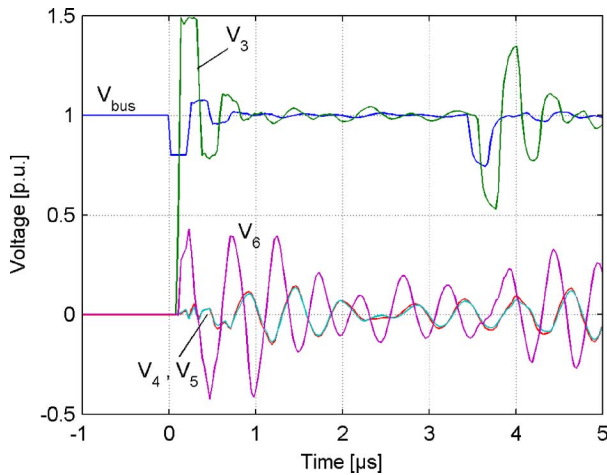


Fig. 22. Transient overvoltages.

shows that the voltage on the busbar end of the 20-m cable increases abruptly from 0 to 0.8 p.u. when the breaker closes. The associated voltage wave on the cable nearly doubles when it meets the transformer (V_3), and a high-frequency oscillation occurs on the cable. The dominating component has frequency $f = 1/(4\tau)$ where τ is the feeding cable (20 m) travel time. The oscillation causes a buildup of an overvoltage on the transformer low-voltage side that exceeds 0.4 p.u. of the busbar voltage. This voltage corresponds to 19 p.u. of the normal (50-Hz) low-frequency voltage.

B. Busbar Connected to the Cable of the Same Length as the Feeder Cable

Even higher overvoltages may result if the transformer feeding cable is energized from another (live) cable of equal length [12]. One situation where this is relevant is shown in Fig. 23, where two generator step-up transformers are fed from the same busbar. When the circuit breaker closes, a voltage wave starts propagating into both cables (with opposite polarity), and the subsequent reflections lead to an oscillating overvoltage on the cable end. The dominating component has frequency $f = 1/(4\tau)$ where τ is the travel time of each of the two cables (20 m).

Fig. 24 shows a time-domain simulation for the case in Fig. 23 without T2, when the first breaker pole (phase C) closes 1 ms before the next pole. The plot shows that the busbar voltage instantly changes from 1 p.u. to 0.5 p.u. and that an oscillating voltage results on the T1 transformer terminal (V_3). As a result,

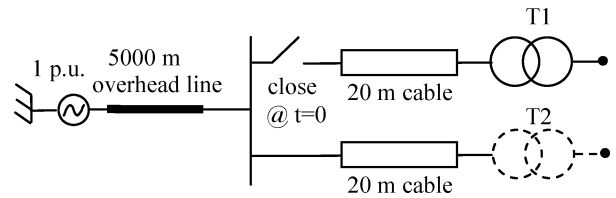


Fig. 23. Transformer energization from the three-phase power system. Closing first breaker pole at $t = 0$.

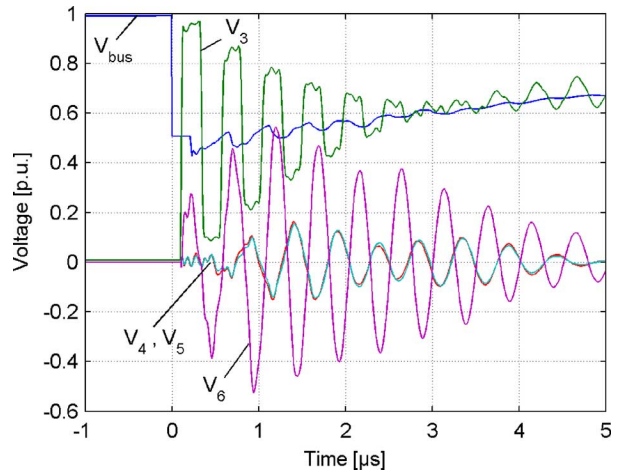


Fig. 24. Transient overvoltages.

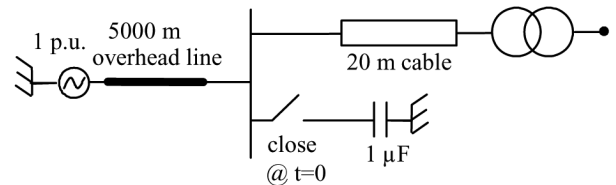


Fig. 25. Capacitor bank energization.

an overvoltage builds up on the low-voltage side of the transformer, giving a maximum voltage of 0.50 p.u. of the busbar voltage.

The following additional results were found.

- 1) If the transformer T2 is included in the simulation, the peak voltage is reduced from 0.50 p.u. to 0.43 p.u. If, in addition, a 30-Ω load is placed on the T2 secondary, the peak voltage drops to 0.41 p.u.
- 2) The overvoltage increases when more cables of the same length (20 m) are connected to the busbar. One additional cable increases the peak voltage from 0.50 p.u. to 0.66 p.u. while two cables gives a peak value of 0.71 p.u.

VI. CAPACITOR BANK ENERGIZATION

The last example case is capacitor bank energization (see Fig. 25). Closing the breaker causes the voltage on the busbar to abruptly drop to zero, not much different from the ground fault situation in Fig. 14. Fig. 26 shows the simulated overvoltages when breaker pole C closes 1 ms before the next pole. It is observed that the voltage on the busbar instantly drops to zero, which gives rise to an oscillating voltage on the far cable end (V_3). This oscillating voltage gives rise to a resonant overvoltage

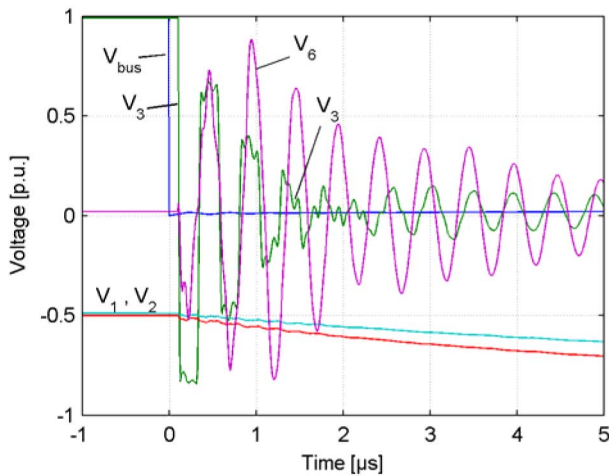


Fig. 26 Transient overvoltages.

on the transformer low-voltage side (V_6), which reaches about 0.9 p.u. of the initial bus voltage. This corresponds to about 43 p.u. of the normal (50 Hz) voltage on the 230-V side.

VII. DISCUSSION

The study was performed on a distribution transformer where the voltage transfer from the high-voltage side to the low-voltage side is maximum at about 2 MHz. Other transformers may have peaks in the voltage transfer at much lower frequencies. As an example, Fig. 27 shows the voltage transfer from high to low for the 410-MVA generator stepup transformer studied in [14]. The primary voltage is 434 kV and the secondary is 21 kV. Clearly, the voltage ratio is particularly high at 50 kHz (0.67) but also considerable at about 170 kHz (0.28). Considering the voltage ratio at 50 Hz ($21 \text{ kV}/434 \text{ kV} = \{0.048\}$), these peaks correspond to voltage ratios of 14 (at 50 kHz) and 6 (at 170 kHz). Thus, transients on the high-voltage side with these characteristic frequencies could lead to excessive overvoltages at the low-voltage side, provided that the input impedance on the high-voltage side is sufficiently high. Assuming a cable propagation velocity of 160 m/ μs , these frequencies would for the situations in Figs. 3–5 occur with cable lengths 800 m (50 kHz) and 235 m (170 kHz).

The practical application of measurement-based black-box transformer models will, of course, require that the transformer be already built and available for measurements. The black-box model approach is therefore not useful for the design of transformers, rather it allows predicting how the transformer may behave in a given electrical system. This could allow for mitigating actions. Install protective devices, make changes to the network layout, or install protective devices. In addition, if a series of identical transformers is manufactured, one only needs to do the measurement/modeling once.

VIII. CONCLUSION

This paper has studied resonant overvoltages on the low-voltage side of a distribution transformer caused by cable-transformer interaction on the high-voltage side. The conclusions are based on measurements in the domains of

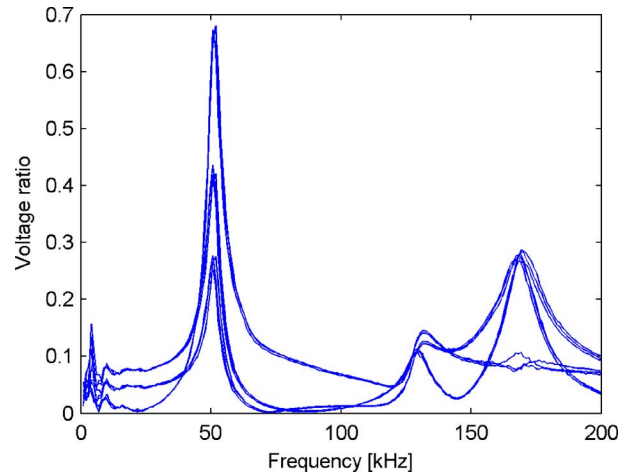


Fig. 27. The 410-MVA generator step-up transformer. Voltage ratio from high (434 kV) to low (21 kV).

frequency and time, and on time-domain simulation by using a black-box model of the transformer.

- 1) Transient events that cause an oscillating overvoltage on a (feeder) cable that connects to the transformer high-voltage side can produce very high overvoltages on the low-voltage side. This requires that the cable characteristic impedance be much lower than the transformer impedance seen in the high-voltage side.
- 2) The highest (resonant) overvoltages occur if the dominating frequency component of the cable voltage matches one of the dominating frequency components of the voltage transfer from the high-voltage side to the low-voltage side. High overvoltages may also result even when a match in frequency does not occur, provided that the impinging transient voltage is sufficiently steep.
- 3) Using a black-box model of the transformer, a measurement of a cable-transformer resonant overvoltage is reproduced with a high degree of accuracy. In practice, a sufficiently accurate model of the adjacent network must also be available.
- 4) Using simulations by the black-box model, three situations are identified which may lead to excessive overvoltages on the low-voltage side: 1) ground fault initiation on feeder cable; 2) transformer energization via feeder cable from a busbar that is connected to several cables; 3) transformer energization via feeder cable from a second cable of about the same length as that of the feeder cable; and 4) capacitor bank energization near the end of the feeder cable.

APPENDIX

MEASUREMENT OF CABLE ADMITTANCE MATRIX

In Section III-B, a high-frequency model was created for a 27-m single-core cable based on measurements. The following describes the adopted measurement procedure.

Using a vector network analyzer (VNA), the voltage transfer between the two cable ends #1 and #2 is measured for two situations: with end #2 open and with end #2 shorted by a 50- Ω resistor, see Fig. 28. Legends A, R, and S refer to the VNA source (S), reference (R), and input (A).

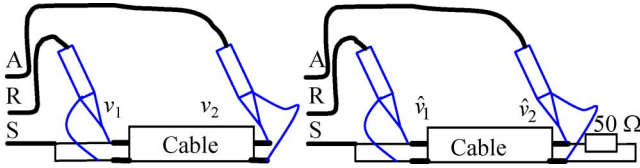
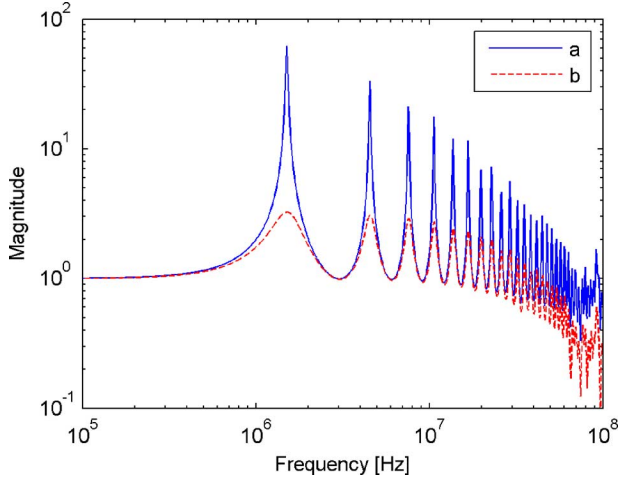


Fig. 28. Transient overvoltages.

Fig. 29. Measured voltage ratios $a = v_2/v_1$ and $b = \hat{v}_2/\hat{v}_1$.

A calibration response is first extracted with the two voltage probes connected to the same point. The inverse of the obtained ratio $f = (v_2/v_1)$ is then used as a multiplier (calibration) for all measured voltage ratios.

The cable nodal admittance matrix has a structure as shown in (4), due to symmetry with respect to the two cable ends

$$\begin{bmatrix} i_1 \\ i_2 \end{bmatrix} = \begin{bmatrix} y_a & y_b \\ y_b & y_a \end{bmatrix} \begin{bmatrix} v_1 \\ v_2 \end{bmatrix}. \quad (4)$$

For the case with end #2 open, we have $i_2 = 0$, which gives

$$y_a = -\frac{y_b}{\left(\frac{v_2}{v_1}\right)}. \quad (5)$$

With the $R = 50 \Omega$ resistor connected to end #2 we obtain for the second row of (4)

$$0 = y_b \hat{v}_1 + \left(y_a + \frac{1}{R}\right) \hat{v}_2. \quad (6)$$

Inserting (5) into (6) gives the final expression (7) for y_b . y_a is finally calculated from (4). Fig. 29 shows the measured responses $a = (v_2/v_1)$ and $b = (\hat{v}_2/\hat{v}_1)$

$$y_b = \frac{\left(\frac{\hat{v}_2}{\hat{v}_1}\right)}{R \left(\left(\frac{\hat{v}_2}{\hat{v}_1}\right) - 1\right)}. \quad (7)$$

ACKNOWLEDGMENT

The author would like to thank K. Ljøkelsøy and O. Rokseth (SINTEF Energy Research) for developing the low-impedance voltage impulse source and for assistance in implementing the measurement setup.

REFERENCES

- [1] A. Morched, L. Marti, R. H. Brierley, and J. G. Lackey, "Analysis of internal winding stresses in EHV generator step-up transformer failures," *IEEE Trans. Power Del.*, vol. 11, no. 2, pp. 888–894, Apr. 1996.
- [2] F. De Leon and A. Semlyen, "A complete transformer model for electromagnetic transients," *IEEE Trans. Power Del.*, vol. 9, no. 1, pp. 231–239, Jan. 1994.
- [3] P. G. Blanken, "A lumped winding model for use in transformer models for circuit simulation," *IEEE Trans. Power Electron.*, vol. 16, no. 3, pp. 445–460, May 2001.
- [4] E. Bjerkan and H. K. Høidalen, "High frequency FEM-based power transformer modeling: Investigation of internal stresses due to network-initiated overvoltages," in *Proc. Int. Conf. Power Systems Transients*, Montreal, QC, Canada, Jun. 19–23, 2005, p. 6.
- [5] M. Popov, L. van der Sluis, R. P. Smeets, and J. L. Roldan, "Analysis of very fast transients in layer-type transformer windings," *IEEE Trans. Power Del.*, vol. 22, no. 1, pp. 238–247, Jan. 2007.
- [6] S. M. H. Hosseini, M. Vakilian, and G. B. Gharehpetian, "Comparison of transformer detailed models for fast and very fast transient studies," *IEEE Trans. Power Del.*, vol. 23, no. 2, pp. 733–741, Apr. 2008.
- [7] A. De, D. Debnath, and A. Chakrabarti, "A study on the impact of low-amplitude oscillatory switching transients on grid connected ehv transformer windings in a longitudinal power supply system," *IEEE Trans. Power Del.*, vol. 24, no. 2, pp. 679–686, Apr. 2009.
- [8] M. Popov, L. van der Sluis, and R. P. P. Smeets, "Evaluation of surge transferred overvoltages," *Elect. Power Syst. Res.*, vol. 78, no. 3, pp. 441–449, 2008.
- [9] M. J. Manyahi and R. Thottappillil, "Transfer of lightning transients through distribution transformers," in *Proc. Int. Conf. Lightning Protection*, Cracow, Poland, Sep. 2–6, 2002, pp. 435–440.
- [10] A. Borghetti, A. Morched, F. Napolitano, C. A. Nucci, and M. Paolone, "Lightning-induced overvoltages transferred through distribution power transformers," *IEEE Trans. Power Del.*, vol. 24, no. 1, pp. 360–372, Jan. 2009.
- [11] G. C. Paap, A. A. Alkema, and L. L. Van der Sluis, "Overvoltages in power transformers caused by no-load switching," *IEEE Trans. Power Del.*, vol. 10, no. 1, pp. 301–307, Jan. 1995.
- [12] B. Storesund, "Resonant overvoltage transients in power systems," Ph.D. dissertation, Norges Tekniske Høgskole, Trondheim, Norway, 1992.
- [13] A. Morched, L. Marti, and J. Ottevangers, "A high frequency transformer model for the EMTP," *IEEE Trans. Power Del.*, vol. 8, no. 3, pp. 1615–1626, Jul. 1993.
- [14] B. Gustavsen and A. Semlyen, "Application of vector fitting to state equation representation of transformers for simulation of electromagnetic transients," *IEEE Trans. Power Del.*, vol. 13, no. 3, pp. 834–842, Jul. 1998.
- [15] B. Gustavsen, "Wide band modeling of power transformers," *IEEE Trans. Power Del.*, vol. 19, no. 1, pp. 414–422, Jan. 2004.
- [16] B. Gustavsen, "Frequency-dependent modeling of power transformers with ungrounded windings," *IEEE Trans. Power Del.*, vol. 19, no. 3, pp. 1328–1334, Jul. 2004.
- [17] M. Tibergh, D. Bormann, B. Gustavsen, and C. Heitz, "Generic and automated simulation modeling based on measurements," in *Proc. Int. Conf. Power Systems Transients*, Lyon, France, Jun. 4–7, 2007, p. 6.
- [18] B. Gustavsen and A. Semlyen, "Rational approximation of frequency domain responses by vector fitting," *IEEE Trans. Power Del.*, vol. 14, no. 3, pp. 1052–1061, Jul. 1999.
- [19] B. Gustavsen and A. Semlyen, "Enforcing passivity for admittance matrices approximated by rational functions," *IEEE Trans. Power Syst.*, vol. 16, no. 1, pp. 97–104, Feb. 2001.
- [20] H. W. Dommel, *ElectroMagnetic Transients Program. Reference Manual. (EMTP Theory Book)*. Portland, OR: Bonneville Power Administration, 1986.
- [21] A. Semlyen and A. Dabuleanu, "Fast and accurate switching transient calculations on transmission lines with ground return using recursive convolutions," *IEEE Trans. Power App. Syst.*, vol. PAS-94, no. 2, pt. 1, pp. 561–575, Mar./Apr. 1975.
- [22] B. Gustavsen and O. Mo, "Interfacing convolution based linear models to an electromagnetic transients program," in *Proc. Int. Conf. Power Systems Transients*, Lyon, France, Jun. 4–7, 2007, p. 6.
- [23] A. J. Schulz, I. B. Johnson, and N. R. Schulz, "Magnification of switching surges," *AIEE Trans. Power App. Syst.*, vol. 77, no. 3, pp. 1418–1425, Apr. 1958.
- [24] B. Gustavsen, "Improving the pole relocating properties of vector fitting," *IEEE Trans. Power Del.*, vol. 21, no. 3, pp. 1587–1592, Jul. 2006.

- [25] D. Deschrijver, M. Mrozowski, T. Dhaene, and D. De Zutter, "Macro-modeling of multiport systems using a fast implementation of the vector fitting method," *IEEE Microw. Wireless Compon. Lett.*, vol. 18, no. 6, pp. 383–385, Jun. 2008.
- [26] B. Gustavsen, "Fast passivity enforcement for pole-residue models by perturbation of residue matrix eigenvalues," *IEEE Trans. Power Del.*, vol. 23, no. 4, pp. 2278–2285, Oct. 2008.
- [27] L. M. Wedepohl and D. J. Wilcox, "Transient analysis of underground power transmission systems; system-model and wave propagation characteristics," *Proc. Inst. Elect. Eng.*, vol. 120, no. 2, pp. 252–259, Feb. 1973.
- [28] A. Morched, B. Gustavsen, and M. Tartibi, "A universal model for accurate calculation of electromagnetic transients on overhead lines and underground cables," *IEEE Trans. Power Del.*, vol. 14, no. 3, pp. 1032–1038, Jul. 1999.
- [29] B. Gustavsen, J. A. Martinez, and D. Durbak, "Parameter determination for modeling system transients—Part II: Insulated cables," *IEEE Trans. Power Del.*, vol. 20, no. 3, pp. 2045–2050, Jul. 2005.

Bjørn Gustavsen (M'94–SM'03) was born in Harstad, Norway, in 1965. He received the M.Sc. and the Dr.ing. degrees from the Norwegian Institute of Technology (NTH), Trondheim, Norway, in 1989 and 1993, respectively.

Since 1994, he has been with SINTEF Energy Research, NTH, where he is currently a Senior Research Scientist. His interests include simulation of electromagnetic transients and modeling of frequency-dependent effects. He spent 1996 as a Visiting Researcher at the University of Toronto, Toronto, ON, Canada, and 1998 at the Manitoba HVDC Research Centre, Winnipeg, MB, Canada. He was a Marie Curie Fellow at the University of Stuttgart, Stuttgart, Germany, from 2001 to 2002.